Using $Si_3N_4/LaAlO_3$ double layer antireflection coatings with improved efficiency for single crystal silicon solar cells

YU-CHIN CHOU[1], YU-LI LIN[2], CHIEN-HUNG WU[2,*], CHENG-YI HSU[1]
[1]*Ph. D Program in Engineering Science, Chung Hua University, Hsinchu, Taiwan, R.O.C*
[2]*Department of Optoelectronics and Materials Engineering, Chung Hua University, Hsinchu, Taiwan, R.O.C*

In this paper, we present highly efficient p-type crystalline silicon solar cells coated with a novel antireflection thin film composed of lanthanum aluminate oxide ($LaAlO_3$). We compared the results of single layer antireflection coatings (SL-ARCs) and double layer antireflection coatings (DL-ARCs). The antireflection thin films were deposited onto solar cells by using plasma-enhanced chemical vapor deposition (PECVD) of silicon nitride (Si_3N_4) and e-beam evaporation of $LaAlO_3$. The deposition method changed the morphology of the $LaAlO_3$ thin film, which contributed to a change of the refractive index. $Si_3N_4/LaAlO_3$ DL-ARCs samples showed higher output performance efficiency than those of Si_3N_4 SL-ARCs samples. Adding a $LaAlO_3$ thin film through this deposition process, increased efficiency by up to 19.56% at AM 1.5G on crystalline silicon solar cells, and demonstrated a 1.46% efficiency gain compared with baseline solar cells with Si_3N_4 SL-ARCs.

(Received October 31, 2022; accepted August 7, 2023)

Keywords: Lanthanum aluminate oxide ($LaAlO_3$), Double layer antireflection coatings (DL-ARCs), Solar cells

1. Introduction

In past research, p-type silicon wafers have been widely used for high-efficiency solar cells because their properties are electrically superior to those of n-type silicon. The minority carrier power of p-type wafers can produce large photocurrents more efficiently than the electron mobility of n-type wafers [1–5]. Antireflection coatings (ARCs) have been used very widely [6–9]. Many researchers have studied double layer ARCs (DL-ARCs) because single layer ARCs (SL-ARCs) can not cover a broad range of the solar spectrum. An effective ARCs is vital for solar cell performance because it ensures a high photocurrent by minimizing reflectance and adds to refraction. Silicon nitride Si_3N_4 films are the most widely used type of films for solar cells; their applications to silicon solar cells have a long history [10–12]. Si_3N_4 has a refractive index in the 1.9-2.4 range [13–18], which is higher than the refractive index of lanthanum aluminate oxide ($LaAlO_3$), which is in the 1.6-2.0 range [19, 20]. In this work, we combined these two materials by using Si_3N_4 DL-ARCs and $LaAlO_3$ thin films that, maintained unbroken ohmic contact with screen-printed industrial silver paste. Here, we propose and demonstrate $Si_3N_4/LaAlO_3$ DL-ARCs for silicon solar cells that have excellent passivation and improve photoelectric conversion efficiency. Numerous experimental characteristics of the prepared samples, including open-circuit voltage (V_{OC}), short-circuit current density (Jsc), fill factor (FF), external quantum efficiency (EQE), and conversion efficiency (η), are presented and discussed.

2. Experimental procedure

Different metal line widths will have different illuminated areas. In this study, we will discuss the photoelectric effect and dark current individually for comparison based on the measurement data results.

From the photoelectric conversion efficiency measurements shown in Table 1 and Fig. 1, the 2.0 mm metal line width is clearly superior to the other metal line widths. Hence, the 2.0 mm metal line width has been selected for the experiment in this study.

Table 1. Overview of cell characterization results with different linewidths on solar cells

Sample	Voc(V)	Jsc (mA/cm^2)	FF %	η (%)
1.7 mm	0.61	38.26	75.15	17.58
1.8 mm	0.61	38.08	73.48	17.08
2.0 mm	0.62	38.94	74.85	18.09
2.1 mm	0.62	38.92	74.77	18.08
2.3 mm	0.61	38.62	74.70	17.74

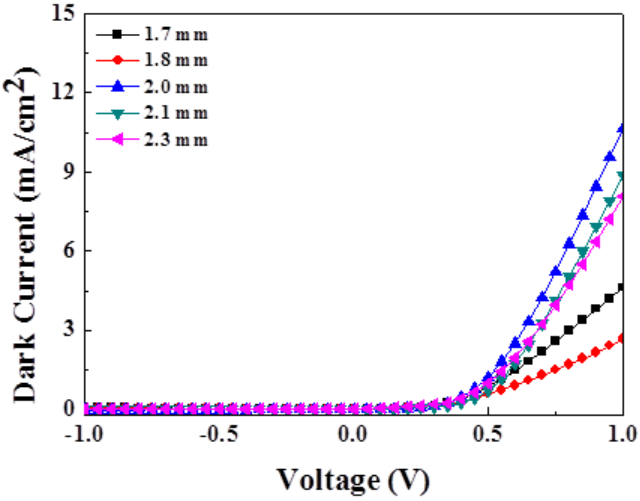

Fig. 1. Dark current of different metal line widths for silicon solar cells (color online)

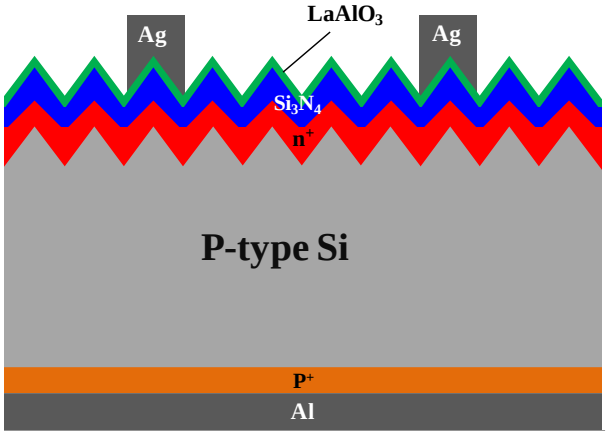

Fig. 2. Configuration of the DL-ARCs passivation and antireflection film structure (color online)

First, p-type Czochralski silicon (100) substrates with a 160 um thickness and a resistivity of 1–2 Ω-cm were cleaned using rrrrrrstandard RCA cleaning processes. Second, pyramidal structures were formed through wet chemical etching using a solution of KOH, isopropyl alcohol (IPA), and deionized water at a temperature of 80 °C for 30 min. Front phosphorus emitters with different sheet resistances were diffused from a $POCl_3$ source at different temperatures. Because cells with a conventional rear junction structure are usually limited by Auger recombination on the front surface field (FSF), n+/p high low junctions were fabricated for the cell emitter through phosphorus diffusion by $POCl_3$. This created a homogenous FSF [21–23]. We used LTPSG oxidation and then etched the backs of the substrates by using a short dilute-HF dip to passivate the surface regions of the lightly doped n+ emitters. LTPSG oxidation was performed through dry oxidation at 800 °C for 5 min in an O_2 ambient after the PSG process. Antireflection (Si_3N_4) films with a thickness of approximately 80 nm were deposited on the front side of the silicon substrates through plasma enhanced chemical vapor deposition (PECVD), and ($LaAlO_3$) films with a thickness of 7.2 –15 nm were deposited through e-beam evaporation on top of the Si_3N_4. Subsequently, Ag paste and Al paste were used as the front contact and rear contact, respectively. Note that the finger space and width of the front contact were 2 mm and 100 nm, respectively. The peak temperature for co firing was 770 °C. Finally, the samples were isolated using a laser. A schematic diagram of the experimental structure of a DL-ARCs is shown in Fig. 2.

The performances levels of the fabricated solar cells were characterized under standard test conditions (25°C and AM 1.5G irradiation at 100 mW/cm^2). Characterization was performed using Quicksun 120CA IV measurement. Measurements of the EQE responses of the bare solar cells, and of the solar cells coated with Si_3N_4/$LaAlO_3$ DL-ARCs were examined for wavelengths ranging from 400 nm to 1100 nm. The EQE responses were measured using the Enli Technology EQE-D-3011. The thickness and refractive index values for Si_3N_4 films and ($LaAlO_3$) thin films were measured using an n&k thin film analyzer (model: 1280, n&K Technology Inc.).

3. Results and discussion

Fig. 3 shows thickness and refractive index measurements of the $LaAlO_3$ thin films. All of the thin films were measured using an n&k thin film analyzer after the thin film had been deposited on Si_3N_4 films with a thickness of 80 nm and a refractive index (n) of 2.0. We measured and compared the optimized reflectivity curves of texted solar cells with SL-ARCs and DL-ARCs as functions of the wavelength λ; results are shown in Fig. 4. The simulated curves fit the measured reflectivity curves of both ARCs structures. Fig. 4 shows that photons with wavelengths in the range between 300 nm and 600 nm had a low reflectance from a solar cell with an SL-ARCs. However, photons in the wavelength range between 600 nm and 1000 nm had low reflectance values from a solar cell with a Si_3N_4/$LaAlO_3$ DL-ARCs. Accordingly, the ARCs can reduce the optical loss and help enhance the conversion efficiency by making use of phase changes and the dependence of the reflectivity on refraction index. An SL-ARC can be non-reflective only at one wavelength, usually at the middle of the visible region. Multiple layers are very low reflection and more effective over the entire visible spectrum [24-25]. Therefore, at almost all regions of the spectrum, the reflectance of a solar cell with a Si_3N_4/$LaAlO_3$ DL-ARCs is lower than that of a solar cell without a $LaAlO_3$ thin film ARCs; however, the bottom of

the reflectance spectrum is almost identical for cells with and without these coatings. In the wavelength range between 600 nm and 700 nm, which is the optimal solar light absorption wavelength range, all solar cells had a low reflectance. However, a $LaAlO_3$ thin film cannot produce a 1.47% efficiency improvement alone. Another benefit is obtained from improved passivation effects introduced by the bottom Si_3N_4 layer, which has a higher refractive index [26].

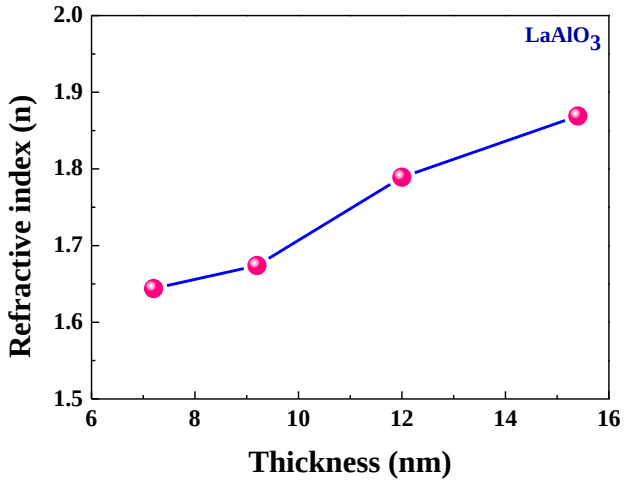

Fig. 3. $LaAlO_3$ thickness and refractive index

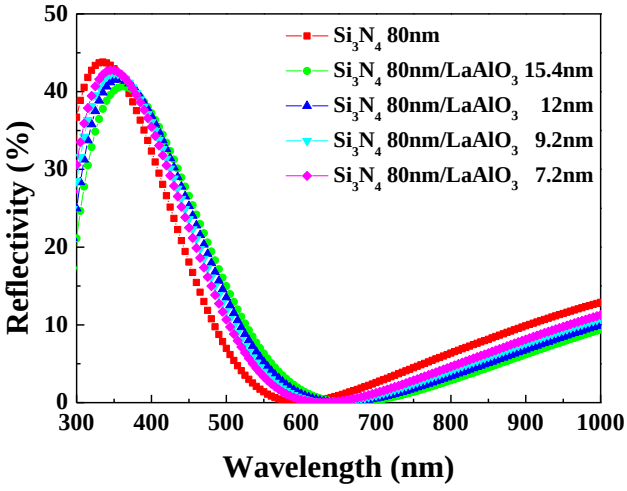

Fig. 4. Measured and simulated reflectivity curves of different thickness ARCs structures (color online)

Fig. 5 shows the dark current of ARCs structures with different thicknesses, Fig. 6 shows the Leakage current of ARCs structures with different thicknesses.

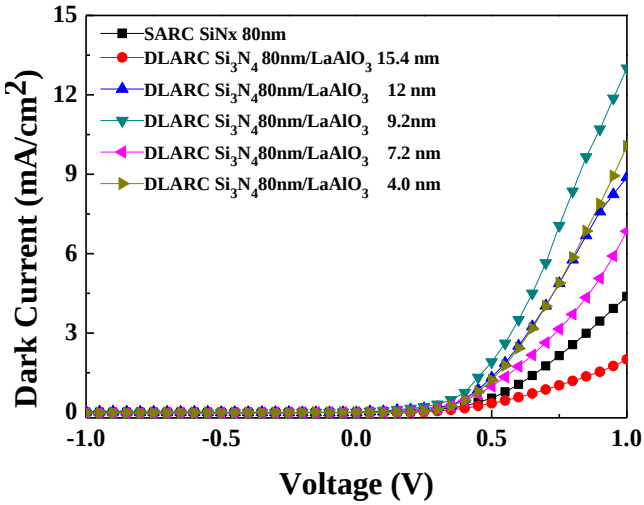

Fig. 5. Dark current of 7.2 to 15.4-nm-thick $LaAlO_3$ films on ARCs structures (color online)

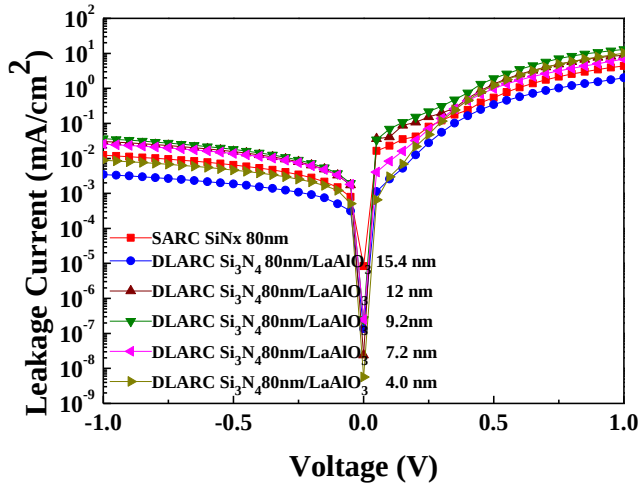

Fig. 6. Leakage current of 7.2 to 15.4-nm-thick $LaAlO_3$ films on ARCs structures (color online)

We used FE-SEM to characterize the surface morphology of the samples. Top views of textured surface are shown in Fig. 7a at 1k resolution and Fig. 7b at 3k resolution. Cross-sectional views are shown in Fig. 7c at 8k resolution and Fig. 7d at 15k resolution. Randomly distributed pyramidal peaks are scarred by small pits, and formed through wet chemical etching by using a solution of KOH/IPA at a temperature of 80 °C for 30 min. The cross-sectional images of the $Si_3N_4/LaAlO_3$ DL-ARCs clearly show the pitted texture of the pyramidal surfaces.

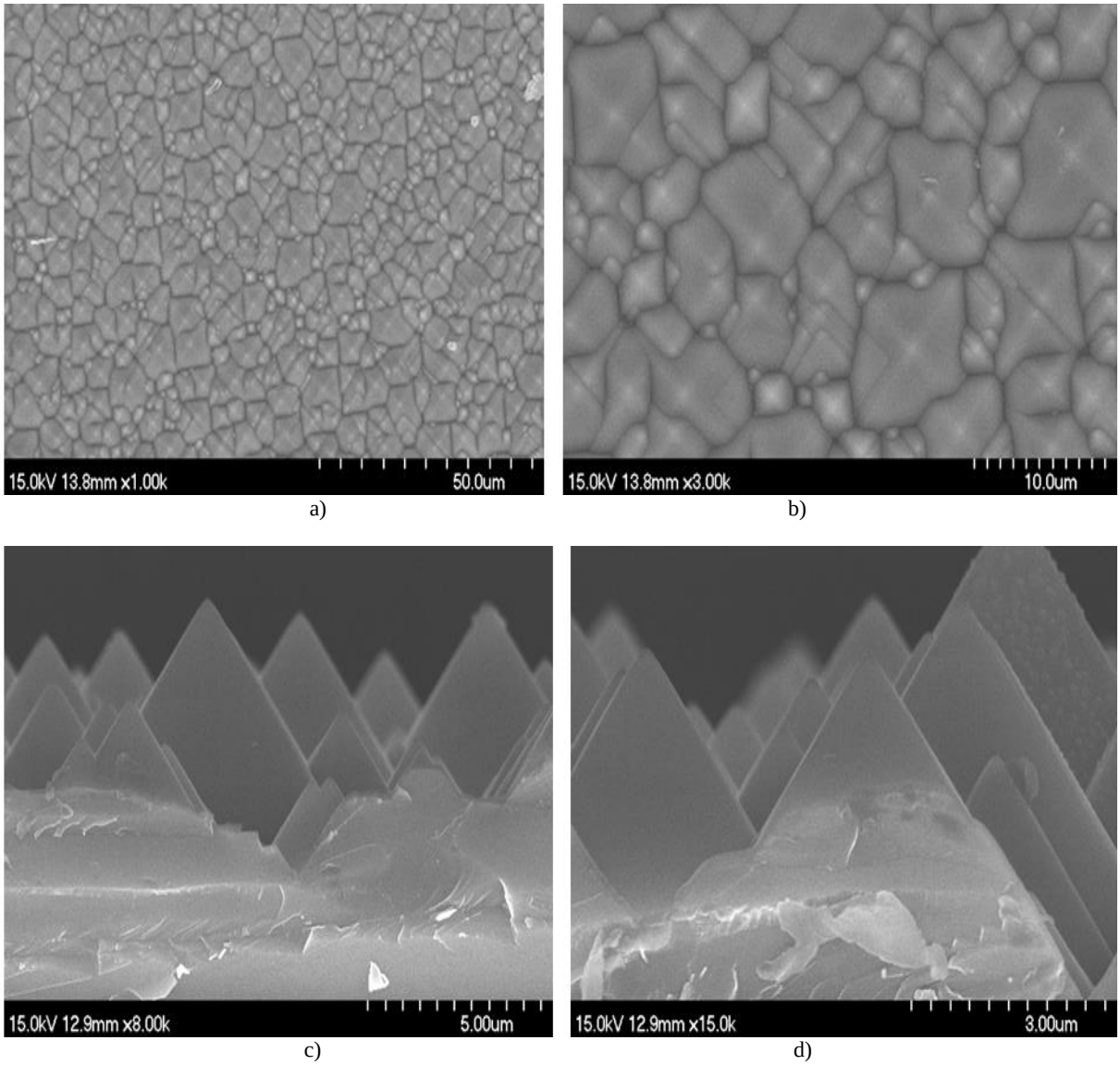

Fig. 7. FE-SEM images of surface texture pyramid substrates a) and b) Top views pyramid texture, c) and d) Cross-sectional views of pitted peaks produced by etching, which are randomly distributed on the pyramids

$$\alpha = \frac{1}{d} \times \ln\left(\frac{1}{T}\right) \quad (1)$$

$$(\alpha \times hv)^2 = B \times (hv - Eg) \quad (2)$$

The optical transmittance spectra of the $LaAlO_3$ films deposited on glass substrates are shown in Fig. 8, and the average transmittance of the $LaAlO_3$ films is more than 85% in the visible range. The transmittance spectrum of each glass substrate is indicated by the horizontal axis. From this equation (1)–(2) as described by [27], in a direct-transition semiconductor, the absorption coefficient, α, and optical band gap (Eg) are related, as follows: where B is a constant, hv is the energy of the incident photon, and T and d are the transmittance and thickness of the thin film, respectively. Fig. 9 shows the optical band gap of 7.2 to 15.4-nm-thick $LaAlO_3$ films. The optical band gap of a $LaAlO_3$ film is approximately 3.82 eV.

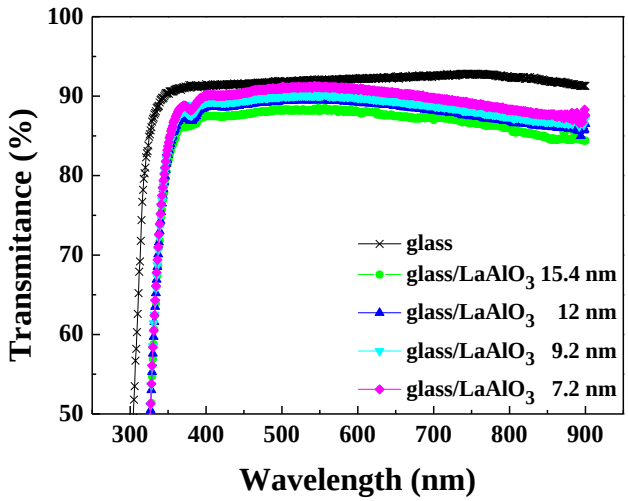

Fig. 8. Optical transmission spectra of 7.2 to 15.4-nm-thick $LaAlO_3$ films on glass substrates (color online)

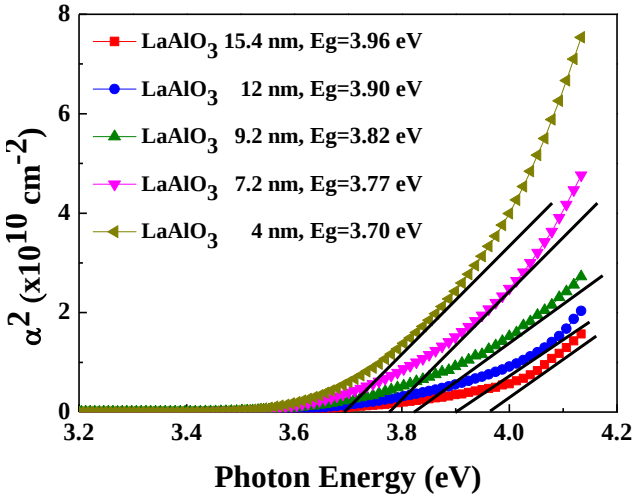

Fig. 9. Optical band gap of 7.2 to 15.4-nm-thick $LaAlO_3$ films (color online)

We calculated the EQE of solar cells fabricated with SL-ARCs and DL-ARCs in the wavelength range of 400 nm–1100 nm, as a function of the wavelength λ to determine the spectral responses of the solar cells. Fig. 10 shows that cells with $Si_3N_4/LaAlO_3$ (7.2 nm and n = 1.64) DL-ARCs have high EQE values in the 400–600 nm wavelength range relative to cells with a Si_3N_4 SL-ARCs. These high EQEs could be caused by the $LaAlO_3$ film increasing the refractive index and reducing the reflectivity of light. More photons are injected into a cell fabricated with a DL-ARCs and possibly the recombination rate is lower at the silicon/DL-ARCs interface, thus increasing the EQE of that solar cells for low wavelengths.

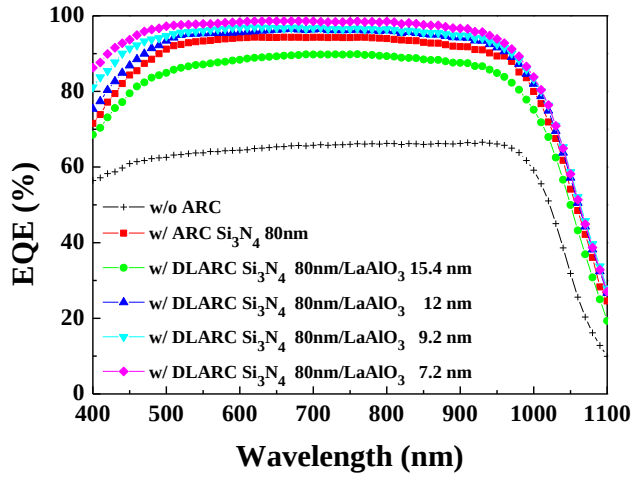

Fig. 10. EQE data of p-type silicon solar cells coated with Si_3N_4 single layer and $Si_3N_4/LaAlO_3$ double layer films in the wavelength range 400–1100 nm (color online)

The current densities of the solar cells fabricated with SL-ARCs and DL-ARCs for the voltage range 0.0–0.7 V are shown in Fig. 11. At AM 1.5G with a cell temperature of 25°C, a high short-circuit current of 41.16 mA/cm^2, open-circuit voltage of 0.62 V, favorable FF of 76.4%, and effective conversion efficiency of 19.56% were achieved. The data indicate that $Si_3N_4/LaAlO_3$ DL-ARCs solar cells have superior output performance to that of Si_3N_4 SL-ARCs cells; in particular, Jsc and conversion efficiency are higher for cells with DL-ARCs. The DL-ARCs improves conversion efficiency by approximately 1.47%. The measurement results are shown in Table 2.

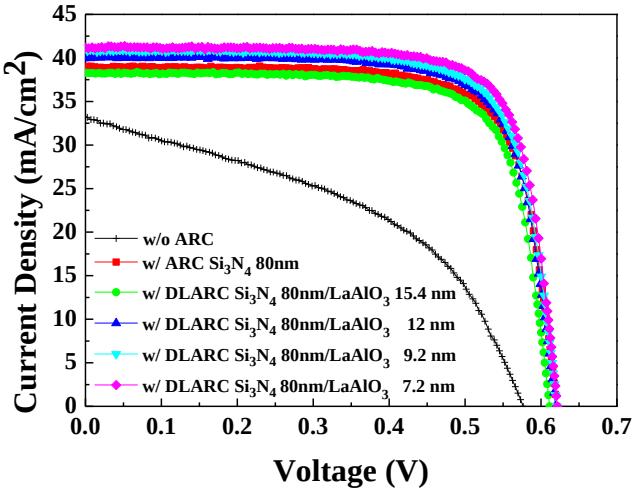

Fig. 11. J–V characteristics of p-type silicon solar cells with SL-ARCs and DL-ARCs (AM 1.5G) (color online)

Table 2. Overview of cell characterization results (AM 1.5G) with different ARCs on p-type solar cells

Process condition	Jsc [mA/cm^2]	Voc [V]	F.F. [%]	Cell eff. [%]
Without ARC	33.18	0.57	44.5	8.53
Si_3N_4 80 nm	38.95	0.62	74.8	18.09
Si_3N_4 80 nm/ $LaAlO_3$ 15.4 nm	38.26	0.61	75.1	17.58
Si_3N_4 80 nm/ $LaAlO_3$ 12 nm	40.07	0.61	75.0	18.62
Si_3N_4 80 nm/ $LaAlO_3$ 9.2 nm	40.86	0.62	74.8	18.99
Si_3N_4 80 nm/ $LaAlO_3$ 7.2 nm	41.16	0.62	76.4	19.56

4. Conclusions

In this paper, we presented a p-type silicon solar cell with a DL-ARCs fabricated by using PECVD to deposit Si_3N_4 and e-beam evaporation to deposit $LaAlO_3$ DL-ARCs. A solar cell with a $Si_3N_4/LaAlO_3$ DL-ARCs has superior output performance, particularly and efficiency. These findings demonstrate the improvement proved by the passivation effect of the bottom Si_3N_4 layer. A $Si_3N_4/LaAlO_3$ (7.2 nm and n = 1.64) DL-ARCs solar cells can improve the refractive index and reduce reflectivity for wavelengths in the range of 600–700 nm. The present research demonstrated the following enhanced values: p-type silicon solar cell efficiency = 19.56%, V_{OC} = 0.62 V, Jsc = 41.16 mA/cm^2, and FF = 76.4%.

References

[1] C. Xiao, D. Yang, X. Yu, X. Gu, D. Que, Solar Energy Materials & Solar Cells **107**, 263 (2012).
[2] K. Lauer, C. Moller, K. Neckermann, M. Blech, M. Herms, T. Mchedlidze, J. Weber, S. Meyer, Energy Procedia **38**, 589 (2013).
[3] J. Perchec, A. Lanterne, T. Michel, S. Gall, R. Monna, F. Torregrosa, L. Roux, Energy Procedia **33**, 18 (2013).
[4] A. Das, A. Rohatgi, 37th IEEE PVSC, 158 (2011).
[5] J. Schmidt, K. Bothe, R. Hezel, 3th Photovoltaic Energy Conversion **3**, 2887 (2003).
[6] A. Amrani, A. Bekhtari, B. Mahmoudi, A. Lefgoum, H. Menari, Vacuum **86**, 386 (2011).
[7] S. Ponce-Alcaintara, C. Caniizo, J. Hofstetter, A. Luque, Spanish Conference on Electron Devices, 33 (2007).
[8] L. Asinovsky, F. Shen, T. Yamaguchi, Thin Solid Films **313**, 198 (1998).
[9] N. Sahouane, A. Zerga, Energy Procedia **44**, 118 (2014).
[10] A. Amrani, A. Bekhtari, B. Mahmoudi, A. Lefgoum, H. Menari, Vacuum **86**, 386 (2011).
[11] J. Hofstetter, C. Cafiizo, S. Ponce-Alcantara, A. Luque, 35th IEEE PVSC, 131 (2007).
[12] M. Winter, H. Holst, P. P. Altermatt, Energy Procedia **38**, 895 (2013).
[13] J. M. Shim, I. H. Kim, D. J. Oh, K. Y. Cho, E. J. Lossen, H.W. Lee, J. Y. Choi1, J. S. Kim, J. E. Shin, S. H. Lee, H. S. Lee, 35th IEEE PVSC, 3604 (2010).
[14] J. Kim, J. Hong, S. H. Lee, J. Korean Phys. Soc. **44**, 479 (2004).
[15] J. Grochowski, M. Mysliwiec, P. Mikulic, W. J. Bock, M. Mietana, Measur. Sci. Technol. **124**(3), 421 (2013).
[16] M. Smietana, W. J. Bock, J. Szmidt, Thin Solid Films **519**, 6339 (2011).
[17] M. G. Hussein, K. Wörhoff, G. Sengo, A. Driessen, Thin Solid Films **515**, 3779 (2007).
[18] M. Junghänel, M. Schädel, L. Stolze, S. Peters, 25th EPSEC, 2637 (2010).
[19] I. Y. K. Chang, J. Y. M. Lee, Appl. Phys. Lett. **93**, 223503-1 (2008).
[20] I. T. W. Weber, N. Audebrand, V. Bouquet, M. Guilloux-Viry, A. Perrin, Solid State Sciences **8**, 606 (2006).
[21] A. Uruena, J. Horzel, S. Singh, I. Kuzma-Filipek, E. Cornagliotti, B. J. John, R. Mertens, J. Poortmans, Energy Procedia **27**, 561 (2012).
[22] C. Mader, R. Bock, J. Schmidt, R. Brendel, Solar Energy Materials & Solar Cells **95**, 1720 (2011).
[23] S. Gatza, K. Bothe, J. Müller, T. Dullweber, R. Brendel, Energy Procedia **8**, 318 (2011).
[24] J. Zhao, Martin A. Green, IEEE Transactions on Electron Devices **38**, 1925 (1991).
[25] S. Y. Lien, D. S. Wuu, W. C. Yeh, J. C. Liu, Solar Energy Materials and Solar Cells **90**, 2710 (2006).
[26] J. F. Lelievre, E. Fourmond, A. Kaminski, O. Palais, D. Ballutaud, M. Lemiti, Solar Energy Materials & Solar Cells **93**, 1281 (2009).
[27] Z. K. Tang, G. K. L. Wong, P. Yu, M. Kawasaki, A. Ohtomo, H. Koinuma, Y. Segawa, Appl. Phys. Lett.. **72**, 3270 (1998).

*Corresponding author: rossiwu@chu.edu.tw